HETEROCLINIC ORBITS, MOBILITY PARAMETERS AND STABILITY FOR THIN FILM TYPE EQUATIONS

RICHARD. S. LAUGESEN & MARY C. PUGH

ABSTRACT. We study the phase space of the evolution equation

$$h_t = -(h^n h_{xxx})_x - \mathcal{B}(h^m h_x)_x,$$

where $h(x,t) \geq 0$. The parameters $n > 0$, $m \in \mathbb{R}$, and the Bond number $\mathcal{B} > 0$ are given. We find numerically, for some ranges of n and m, that perturbing the positive periodic steady state in a certain direction yields a solution that relaxes to the constant steady state. Meanwhile perturbing in the opposite direction yields a solution that appears to touch down or 'rupture' in finite time, apparently approaching a compactly supported 'droplet' steady state. We then investigate the structural stability of the evolution by changing the mobility coefficients, h^n and h^m. We find evidence that the above heteroclinic orbits between steady states are perturbed but not broken, when the mobilities are suitably changed. We also investigate touch–down singularities, in which the solution changes from being everywhere positive to being zero at isolated points in space. We find that changes in the mobility exponent n can affect the *number* of touch–down points per period, and affect whether these singularities occur in finite or infinite time.

1. INTRODUCTION

We study the evolution equation

$$h_t = -(h^n h_{xxx})_x - \mathcal{B}(h^m h_x)_x, \tag{1.1}$$

where $n > 0, m \in \mathbb{R}$, and the Bond number $\mathcal{B} > 0$. This is the one-dimensional version of

$$h_t = -\nabla \cdot (f(h)\nabla \Delta h) - \nabla \cdot (g(h)\nabla h) \tag{1.2}$$

with $f(h) = h^n, g(h) = -\mathcal{B}h^m$. Such equations have been used to model the dynamics of a thin film of viscous liquid. The air/liquid interface is at height $z = h(x,y,t) \geq 0$ and the liquid/solid interface is at $z = 0$. The one dimensional equation (1.1) applies if the liquid film is uniform in the y direction.

The fourth order term in equation (1.2) reflects surface tension effects [22, 24]. Typically $f(h) \sim h^n$ as $h \to 0$, for some $1 \leq n \leq 3$, and this motivates our choice of $f(h) = h^n$ in (1.1). Notice also that the fourth order term $-(h^n h_{xxx})_x$ in (1.1) is linearly stabilizing around the constant steady state.

The second order term in (1.2) can reflect gravity, van der Waals interactions, thermocapillary effects or the geometry of the solid substrate. Typically $g(h) \sim \mathcal{B}h^m$ as $h \to 0$, for some $m, \mathcal{B} \in \mathbb{R}$. Choosing $\mathcal{B} > 0$, the second order term $-\mathcal{B}(h^m h_x)_x$ in (1.1) is linearly destabilizing around the constant steady state (it is like a backwards heat equation term). The competition between this destabilizing term and the stabilizing fourth order term generates interesting dynamics. The dynamics are less interesting when $\mathcal{B} \leq 0$, which we do not consider in this paper.
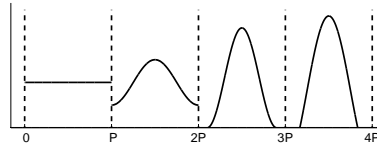

FIGURE 1.   Four types of steady state. The x-axis is space. The two steady states on the left extend smoothly to be P-periodic. The two on the right have less regularity and are called 'droplet' steady states. The third profile has zero contact angles and the fourth has nonzero contact angles. Both have length less than P, and so are possible long–time limits of a P-periodic solution of the evolution equation.

Definitions. In [17] we studied the four types of steady state shown in Figure 1. There are two smooth types of steady state: constant and (nonconstant) positive periodic. Two other types of steady state with lower regularity are the 'droplet' steady states. They either have zero contact angles or nonzero contact angles.

Positive periodic steady states are classical solutions of the steady state equation (that is, (1.1) with $h_t \equiv 0$). When we refer to the period, P, of a nonconstant positive periodic steady state, we mean the shortest period. The area, A, is then defined to be $\int_0^P h_{ss}\, dx$. Constant steady states have no shortest period, however we will always discuss them in the context of an initial value problem, for which the period and area are unambiguous. Because constant steady states are periodic steady states of the most trivial kind, in the following when we refer to positive periodic steady states we implicitly mean *nonconstant* ones.

A droplet steady state h_{ss} is by definition positive on some interval (a, b) and zero elsewhere, with $h_{ss} \in C^1[a, b]$; h_{ss} satisfies the steady state equation classically on (a, b), and has equal acute contact angles: $0 \leq h'_{ss}(a) = -h'_{ss}(b) < \infty$. (Throughout the paper, if a function has only one independent variable then we use $'$ to denote differentiation with respect to that variable: $h'_{ss} = (h_{ss})_x$.) The area, A, of a droplet is $A = \int_a^b h_{ss}\, dx$ and the length is $b - a$.

As suggested by Figure 1, we are interested in droplet steady states whose length is equal to or shorter than P. This is because we want to study the initial value problem with positive initial data of period P and area A. A steady droplet with area A whose length is less than or equal to P must be considered as a possible long–time limit of the evolution. A 'configuration' of droplet steady states is defined to be a collection of steady droplets whose supports are disjoint. Any such configuration whose total area is A and whose total length is less than P must also be considered as a possible long–time limit of the initial value problem.

Background, and Overview of Paper. In [18] we proved linear stability results for steady states. Section 2 summarizes these results by means of a family of bifurcation diagrams, and also presents a weakly nonlinear stability analysis.

Our investigations in the rest of the paper are guided by the study of a dissipated energy for the evolution equation. This energy is defined for P-periodic functions ℓ on $\mathbb{R}$ to be

$$\mathcal{E}(\ell) = \int_0^P \left[\frac{1}{2}(\ell'(x))^2 - \frac{\mathcal{B}}{(m-n+1)(m-n+2)} \ell^{m-n+2}(x) \right] dx. \qquad (1.3)$$

This energy is strictly dissipated: if $h(x,t)$ is a smooth, spatially P-periodic solution of (1.1) then $\frac{d}{dt}\mathcal{E}(h(\cdot,t)) \leq 0$, with equality if and only if h is a steady state of the evolution (cf. [19, §2.1]). Like the evolution equation, the energy $\mathcal{E}(\ell)$ is insensitive to translation in x.

The evolution (1.1) describes *gradient flow* for the energy $\mathcal{E}$, with respect to the following weighted H^{-1} inner product. Let $h(x,t)$ be a positive smooth function that is P-periodic in x. For each t, define an inner product on the space of continuous P-periodic functions with mean value zero, by

$$\langle u, v \rangle := \int_0^P U'(x)V'(x)h(x,t)^n \, dx, \qquad (1.4)$$

where U and V are P-periodic, have zero mean, and are determined from u, v, and $h(\cdot,t)$ via: $u = (h^n U_x)_x$ and $v = (h^n V_x)_x$. Then the evolution equation (1.1) is equivalent to:

$$\frac{\delta\mathcal{E}}{\delta\phi} = \lim_{s\to 0} \frac{\mathcal{E}(h+s\phi) - \mathcal{E}(h)}{s} = -\langle h_t, \phi \rangle$$

for all continuous P-periodic ϕ having mean value zero. The variation of the energy is most negative in the direction $\phi = h_t$, so that the evolution equation for $h(x,t)$ describes flow by steepest descent on the energy surface of $\mathcal{E}$, with respect to the time- and solution-dependent inner product (1.4). The steady states are critical points of this energy surface, with unstable steady states being saddle points and asymptotically stable steady states being minima. The above gradient flow formulation was observed by Fife [11] and by Taylor and Cahn [27]. Gradient flow ideas for related equations have been used in [2, 30, 26]. We refer the readers to Fife's survey article on pattern formation in gradient systems [12].

Note that the perturbing function ϕ is required to have mean value zero because the equation (1.1) preserves area, under periodic (or Neumann) boundary conditions. That is, given initial data with area A, only those points on the energy landscape representing functions with the *same* area will be accessible to the solution.

In [19] we studied the energy landscape of (1.3) under the evolution (1.1), and conjectured the existence of heteroclinic orbits from certain high-energy steady states to certain low-energy steady states. In this paper we find such orbits numerically, in Section 3.1, by computing solutions of the initial value problem for (1.1). We further ask how robust these orbits are under changes in the mobility coefficients h^n and h^m. If we vary m and n while keeping $m - n$ fixed, the steady states and their energy stability are unchanged (since $\mathcal{E}$ depends only on $m - n$). We find that the heteroclinic orbits are perturbed but do not break, when m and n are varied in this way.

In Sections 3.2 and 3.3 we study orbits from a positive periodic steady state to a droplet steady state. Here the long–time limit is not strictly positive, raising the question of whether or not the solution will be positive (and hence classical) for all time, or whether there will be 'touch–down singularities', places and times at which the solution is zero (and hence weak). We find that the value of $m - n$ can affect whether touch–down singularities are present (§3.2), as well as the number of such singularities that arise per period (§3.3).

Section 4 presents a detailed numerical study of the evolution equation (1.1), for initial data close to a steady state and for a number of different exponents n and m. Our stability and energy level results from [18, 19] lead to many predictions for the behavior of the solutions, both short and long time, and these predictions are borne out by our simulations. However there are also situations for which we can make no prediction, and where the numerically observed behavior is rather intriguing.

In Section 5 we sum up the paper. Appendix A discusses our numerical methods and gives the specific parameters used in the simulations.

2. Bifurcation diagrams and weakly nonlinear analysis

First, we rescale the equation and present the weakly nonlinear analysis near the constant steady state. Then, we present bifurcation diagrams that summarize the linear stability of constant steady states and positive periodic steady states.

2.1. Non-dimensionalizing the equation.
A solution of the evolution (1.1) reflects five free parameters: m, n, $\mathcal{B}$, the period P, and the area A. First, we rescale space, time, and the solution itself:

$$\zeta = \frac{x}{P}, \quad t' = P^{n+4} A^{-n} t, \quad \text{and} \quad \frac{A}{P} \eta(\zeta, t') = h(x, t).$$

The rescaled solution, η, has period 1 and area 1 and satisfies the rescaled evolution equation

$$\eta_{t'} = -(\eta^n \eta_{\zeta\zeta\zeta})_\zeta - E(\eta^m \eta_\zeta)_\zeta \tag{2.1}$$

where

$$E = \mathcal{B} A^{q-1} P^{3-q} \quad \text{and} \quad q := m - n + 1. \tag{2.2}$$

In the simulations that follow, in Sections 3 and 4, we always take $P = A = 1$. Then the original evolution equation (1.1) and the rescaled evolution (2.1) are identical, and $\mathcal{B} = E$ is the bifurcation parameter. So in the following we will refer to h, $\mathcal{B}$ and equation (1.1), rather than to η, E and equation (2.1).

2.2. Weakly nonlinear analysis.
For the weakly nonlinear analysis, we consider values of $\mathcal{B}$ such that the constant steady state has one mode which is barely linearly stable or is barely linearly unstable. Since all other modes are strongly damped, this provides a separation of timescales, allowing one to find a reduced representation of the PDE in terms of an ODE governing the amplitude of the unstable mode (cf. [21, §5.1]).

Linearizing equation (1.1) about $\overline{h} = 1$ and considering perturbations $\epsilon \cos(k 2\pi x + \phi)$, one finds a critical value $k_c = \sqrt{\mathcal{B}}/(2\pi)$. If $k_c \leq 1$ then there are no unstable modes. If $k_c > 1$ then there is a finite collection of linearly unstable modes. We assume $\mathcal{B} = 4\pi^2 + Q\delta^2$ where $Q = \pm 1$. Here, δ is a small parameter and varying δ results in k_c moving through the wave number 1. We then introduce a slow time-scale $\tau = \delta^2 t$ and expand the solution in orders of δ: $h(x, \tau) =$

$1 + \delta\, h_1(x,\tau) + \delta^2 h_2(x,\tau) + O(\delta^3)$. For simplicity, we assume the solution is even. By the usual arguments, $h_1(x,\tau) = A(\tau)\cos(2\pi x)$ and $h_2(x,\tau) = B(\tau)\cos(4\pi x)$. Putting this ansatz into the evolution equation (1.1) and expanding in orders of δ, we find there are no $O(1)$ or $O(\delta)$ terms. At $O(\delta^2)$ one determines the amplitude $B(\tau)$ in terms of $A(\tau)$. At $O(\delta^3)$ one finds that $A(t)$ satisfies

$$\frac{dA}{d\tau} = 4\pi^2 Q A(\tau) - \kappa A(\tau)^3, \quad \text{where} \quad \kappa = \frac{8}{3}\pi^4 (q-1)(7/4 - q)$$

and we recall $q = m - n + 1$. The dynamics of the amplitude $A(\tau)$ depend on the signs of the Landau constant κ and of the linear term. If $\kappa > 0$ then for $Q = 1$ the steady state $A_0(\tau) \equiv 0$ is linearly unstable and $A(\tau)$ saturates to the linearly stable steady state $A_c(\tau) \equiv \sqrt{\sigma/\kappa}$. This corresponds to a supercritical bifurcation. If $\kappa < 0$ then for $Q = -1$ the steady state $A_0(\tau) \equiv 0$ is linearly stable and the steady state $A_c(\tau) \equiv \sqrt{-\sigma/\kappa}$ is linearly unstable. This corresponds to a subcritical bifurcation. And so,

$1 < q < 7/4 \Longrightarrow$ *supercritical bifurcation*, $\quad q < 1$ or $7/4 < q \Longrightarrow$ *subcritical bifurcation*.

Subcritical bifurcations are often seen in systems that can have finite-time pinching (rupture) singularities *e.g.* [2, §3.2], [23, §IV]. The above weakly nonlinear analysis was done for $q = -3$ in [30, §2.3].

2.3. Bifurcation diagrams.
Figure 2 gives bifurcation diagrams for representative q-values. To construct a bifurcation diagram, we fix a value for $q = m - n + 1$ and then compute a collection of positive periodic steady states h_{ss} all with period 1 and area 1. Each steady state satisfies the steady version of (1.1) for some value of $\mathcal{B}$. We then plot the amplitude of h_{ss} versus the bifurcation parameter $\mathcal{B}$. We use our linear stability results from [18] to determine whether to plot with solid lines (linearly stable) or with dashed lines (linearly unstable). The horizontal axes of these diagrams show the linear stability of the (zero-amplitude) *constant* steady state. These stability results are all with respect to zero-mean perturbations having the same period as the steady state. Perturbations with longer period always lead to linear instability [18].

Figure 2 provides nine graphs to help the reader visualize the dependence of the diagram on q. (In what follows, we do not discuss simulations for $q = 1.76$ or 1.775.) By examining the bifurcation diagrams near the point $(4\pi^2, 0)$, one observes the subcritical and supercritical bifurcations predicted by the weakly nonlinear stability analysis.

The bifurcation diagrams also encode existence information for steady states. Consider Figure 2b for $q = 1/2$. It starts at $\mathcal{B} = 33.07$ and ends at $\mathcal{B} = 4\pi^2$ with amplitude zero. If $\mathcal{B}$ equals 31 or 42, for example, then there is no (nonconstant) positive 1-periodic steady state with area 1. If $\mathcal{B} = 34$ then there is a unique nonconstant positive 1-periodic steady state with area 1. The monotonicity of the bifurcation diagram corresponds to uniqueness of the positive periodic steady state with specified period and area, if it exists. If the diagram is non-monotonic, there may be zero, one, or two (nonconstant) positive 1-periodic steady states with area 1, depending on the value of $\mathcal{B}$. Non-monotonicity holds for $q \in (7/4, 1.794)$ where 1.794 approximates a criticial exponent q^* (see [17, §5.1]).
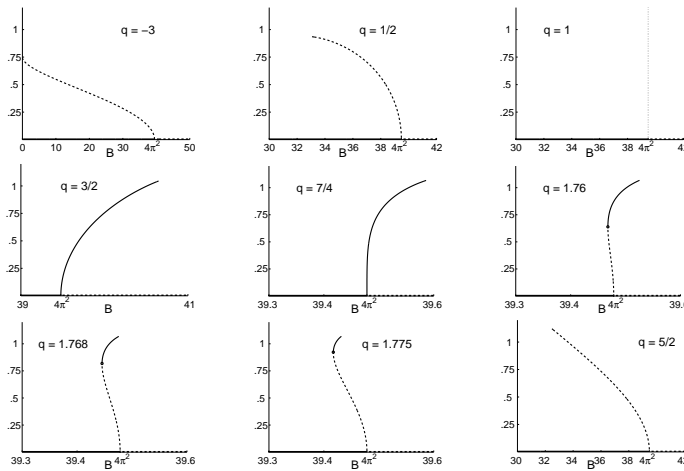
FIGURE 2.   The horizontal axis is the bifurcation parameter $\mathcal{B}$
and the vertical axis is the amplitude of the steady state, $(h_{max} -
h_{min})/2$. Dashed: linearly unstable; dotted: linearly neutrally
stable; solid: linearly stable. There is an interval of $\mathcal{B}$ values for
which (nonconstant) positive periodic steady states exist. They
are linearly unstable for $q \in (-\infty, 1)$, are linearly stable for $q \in
(1, 7/4)$, and are linearly unstable for $q \in (q^*, \infty)$ where $q^* \approx 1.794$.
For $q \in (7/4, q^*)$, there can be two such steady states, one linearly
unstable and one linearly stable. One can prove that for $q \leq -1$,
as $B \to 0$ the amplitude of the solution converges to $3/4$. The
solid and dashed lines on the horizontal axis represent the linear
stability of the constant (zero amplitude) steady states.

3. DYNAMICS: THE EFFECT OF CHANGING THE MOBILITY EXPONENTS, n AND m

Here we vary n and m in $h_t = -(h^n h_{xxx})_x - \mathcal{B}(h^m h_x)_x$ while keeping $m - n$
fixed. We call the exponents n and m mobility parameters, since they determine
the diffusion coefficients of the fourth and second order terms in the equation. Since
$q = m - n + 1$ is being kept fixed, the energy landscape and steady states of the
evolution are unchanged. The linear stability properties of the constant and positive
periodic steady states are also unchanged [18]. We ask three questions about the
effects of changing n and m in this way:

(1) Can a heteroclinic orbit between steady states be *broken*, or is it merely
    perturbed?
(2) Can the *type* of a singularity be altered (*e.g.* from finite-time to infinite-
    time)?
(3) Can the *number* of singularities be altered (*e.g.* from one to two per period)?

In the following, we are interested in heteroclinic orbits between smooth steady
states and between smooth steady states and droplet steady states. For this reason,
we take $q < 1$ or $q > 7/4$ since for these q-values one can find linearly unstable
positive periodic steady states (see Figure 2). For specificity, we present results
for $q = 5/2$ simulations. We observed similar phenomena for other values of q.

We did not have to work hard to capture the $t \to \infty$ limit and so we expect that our infinite–time limits are not saddle points. The reader who is curious about infinite–time limits that are saddle points should refer to [20, 6, 10].

3.1. **Perturbing heteroclinic orbits between smooth steady states.** First we fix $q = 5/2$ and find a positive periodic steady state $h_{\rm ss}$ having period 1 and area 1. It is a steady state of (1.1) with $\mathcal{B} = 35.32$ and is linearly unstable, by bifurcation diagram 2i. We perturb $h_{\rm ss}$, computing the solution of $h_t = -(hh_{xxx})_x - \mathcal{B}(h^{5/2}h_x)_x$ with initial data $h_{\rm ss} + .001h_{\rm ss}''$. We find that the local minimum of the solution remains fixed in space and, after a short transient, it increases to 1. The maximum behaves similarly, decreasing to 1. That is, the solution relaxes to the constant steady state as $t \to \infty$. This suggests there is a heteroclinic orbit connecting the positive periodic steady state to the constant steady state.

We then vary the mobility coefficients, taking $n = 0, 1, 2,$ and 3, choosing m in turn so that $q = m - n + 1 = 5/2$. That is, we compute solutions for the four evolution equations, all with the same initial data. We find that all four solutions relax to the constant steady state: the apparent heteroclinic orbit is not broken by this change in mobility.

But there are differences attributable to the change in mobilities: in Figure 3 we plot $h_{min}(t)$ and $h_{max}(t)$ versus time for the four solutions. The larger the exponent n, the longer it takes for the solution to relax to the constant steady state. We explain this as follows. Because the mean value of $h(\cdot, t)$ is 1, $h_{min}(t) < 1$ for all t and $h_{max}(t) > 1$ for all t. Thus at each time, for x near the minimum point one has $1 = h(x,t)^0 > h(x,t)^1 > h(x,t)^2 > h(x,t)^3$, suggesting that the larger $n = 0, 1, 2, 3$ is, the slower the fourth-order diffusion will be (near the minimum). Similarly, since the maximum is larger than 1 we have $1 = h(x,t)^0 < h(x,t)^1 < h(x,t)^2 < h(x,t)^3$ near the maximum, suggesting that the larger n is, the faster the diffusion will be (near the maximum). This conflict of timescales appears to be mediated through the conservation of mass: the solution moves as slowly as its slowest part. Thus the larger n is, the slower the diffusion.

3.2. **Changing the type of singularities.** Above, we considered a heteroclinic orbit from a positive periodic steady state to a constant steady state. Perturbing in the opposite direction, we find the solution with initial data $h_{\rm ss} - .001h_{\rm ss}''$ appears to converge towards a droplet steady state. This raises the question of whether the solution will be positive and hence classical its entire time of existence, or whether there might be times at which the solution is zero at some points, in which case the solution is weak.

The equation $h_t = -(h^n h_{xxx})_x$ has been the study of extensive computational work on how the exponent n affects the spatial structure of singularities and whether they occur in finite or in infinite time [3]. Simulations suggest there is a critical exponent $1 < n_0 < 2$ such that if $n > n_0$ then solutions are positive for all time while solutions can touch down in finite time if $n < n_0$. Here, we seek the analogous critical exponent $n_0(q)$.

The mobility coefficients in $h_t = -(h^n h_{xxx})_x - \mathcal{B}(h^m h_x)_x$ can affect whether a positive solution can become zero somewhere in finite time. For example, if $7/2 < n \leq m < n + 2$ then it has been proved that the solution stays positive for all $t > 0$, by [4, §4.2]. Note that $m < n + 2$ means $q < 3$. For $q > 3$, Bertozzi and Pugh [4] conjecture that solutions could blow up, with $\|h(\cdot, t)\|_{H^1} \to \infty$ in finite
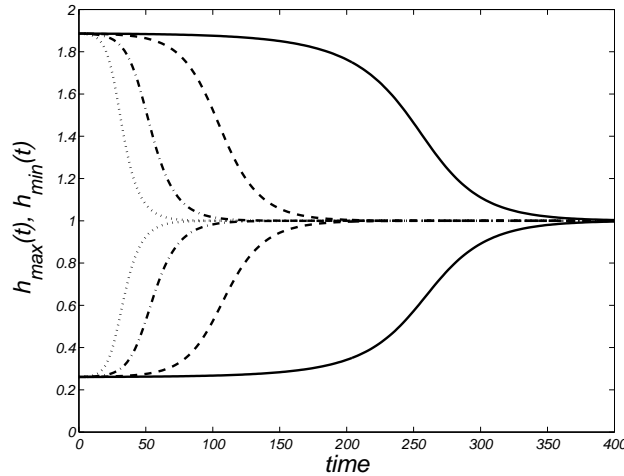
FIGURE 3. $q = 5/2$. We compute solutions of the evolution equation where the initial data is fixed and (m, n) equals $(3/2, 0)$, $(5/2, 1)$, $(7/2, 2)$, and $(9/2, 3)$. We then plot $h_{max}(t)$ and $h_{min}(t)$ versus t for the four solutions: dotted $n = 0$, dot-dashed $n = 1$, dashed $n = 2$, solid $n = 3$. The larger n is, the slower h_{max} and h_{min} converge to 1.

time. However, the methods of [5] do apply to show that that if $n > 7/2$ then the solution remains positive for as long as it exists. Thus the critical exponent for touch–down singularities satisfies $n_0(q) \leq 7/2$.

For $q = 1$ and $n = 1$, Goldstein et al. [13, §4] presented simulations suggesting a finite-time singularity is possible. Bertozzi and Pugh [4] presented numerical simulations for $q = 1$ and $n = 3$ in which the solutions remain positive for all time, though they appear to converge to droplets as $t \to \infty$. So it seems that $1 < n_0(1) < 3$.

For $q = 5/2$, we find that when $n = 1$ the solution appears to touch down in finite time, implying $1 \leq n_0(5/2) \leq 7/2$. To further approximate $n_0(5/2)$, we performed simulations with a variety of n-values, all with the initial data $h_{\mathrm{ss}} - .001 h''_{\mathrm{ss}}$. Our findings suggest

$$1.65 < n_0(5/2) < 1.6625.$$

The evidence is presented in Figure 4, where we plot $\log_{10} h_{min}(t)$ versus t. If $h_{min}(t)$ is decreasing at an exponential rate then the graph will be linear. If $h_{min}(t)$ is decreasing to zero in finite time with an algebraic rate then the graph will drop to $-\infty$ at that time with a vertical slope. From Figure 4, if $n = 2$ then h_{min} decreases monotonically in time, eventually decreasing with an exponential rate. For $n = 1.75, 1.7, 1.675$, and 1.6625, h_{min} decreases and then increases, ultimately decreasing with an exponential rate. (We ran the simulations many decades beyond those shown, to verify the exponential rate of decrease.) The solutions with $n < 1.6625$ appear to be touching down in finite time. However the $n = 1.6625$ simulation gives a note of caution; it is possible that the simulations with $n < 1.6625$ would run until h_{min} became quite small but would then increase
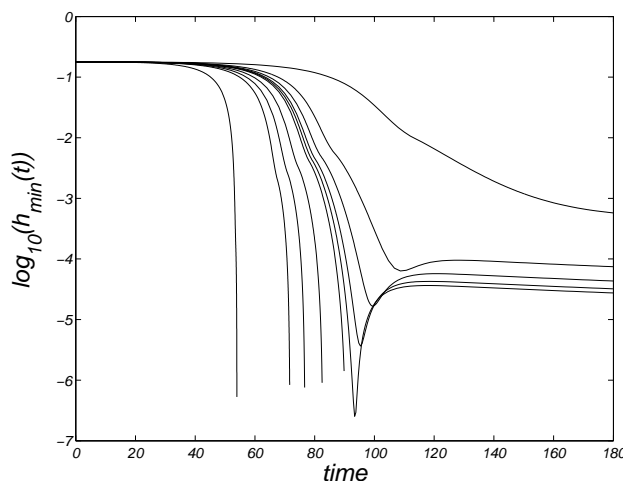
FIGURE 4.   We fix the initial data and compute the solution of
(1.1) where $q = 5/2$ and $n = 1$, 1.25, 1.5, 1.55, 1.6, 1.65, 1.6625,
1.675, 1.7, 1.75,and 2. We plot $\log_{10}(h_{min}(t))$ versus t. (In the
plot, the graphs move rightwards as n increases.) For the first five
values of n the graph appears to go to $-\infty$ in finite time.

somewhat and ultimately decrease exponentially. We stopped our simulations when
the solutions were no longer numerically resolved (see §A.4–A.5).

To check that the bound on $n_0(5/2)$ is not dependent on our choice of initial
data, we chose ten large random perturbations with $||v||_\infty = .178 \sim h_{\text{ss}min}$. Seven
of the resulting solutions relaxed to the constant steady state and three appeared
to touch down in finite time. We then fixed those initial data and varied the value
of n. For all three initial data, we found the above upper and lower bounds on
$n_0(5/2)$.

The critical exponent $n_0(q)$ certainly depends on the value of q. For example,
for $q = 1/2$, we observe similar phenomena to the $q = 5/2$ case presented in Figure
4, and conclude

$$1.8 \le n_0(1/2) < 1.85.$$

To sum up, we find that changing the mobility coefficients (m, n) while keeping
the energy landscape fixed can change the nature of trajectories across the energy
landscape: if $n > n_0(q)$ then the solution is smooth and classical at all times, while
if $n < n_0(q)$ then there can be times when the solution is weak.

3.3. **Splitting singularities.** Here we demonstrate another effect of changing the
mobility: a solution that evolves towards touch–down at just one local minimum
(per period) can change into a solution with two local minima (per period).

q = 5/2. If $n > 0$ and $q = 5/2$ then positive periodic smooth solutions of (1.1)
remain bounded in H^1 for as long as they exist, since $\|h(\cdot,t)\|_{H^1} \le M < \infty$ by
[4]. Because the energy $\mathcal{E}$ decreases in time, we expect that these solutions will
converge to a steady state, as $t \to \infty$. The positive periodic steady state is linearly
unstable, and so we expect solutions to converge either to the constant steady state
or to a configuration of steady droplets.

We take the same initial data as in §3.2. There, we found that if $n < 1.6625 \approx n_0(5/2)$ then solutions appear to touch down in finite time, and if $n > n_0(5/2)$ then touch–down is in infinite time. Here we investigate the nature of the touch–down more closely.

We find for $n = 1$ that the solution touches down in finite time at one point per period, consistent with a long–time limit of one droplet per period (left side of Figure 5). For $n = 2$ the solution appears to be positive at all times and to touch down at two points per period in the long–time limit (right side of Figure 5). This is consistent with a long–time limit of two steady droplets per period. But it is impossible to contain two zero contact angle steady droplets in an interval of length 1 (see §A.6.1). In fact, we find that the small 'proto-droplet' flanked by the local minima is actually draining, with its maximum decreasing to zero like $t^{-.4024}$.
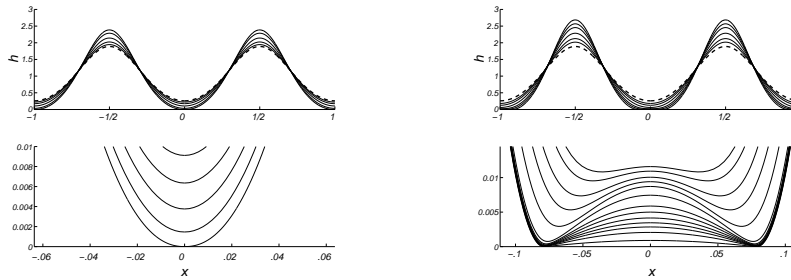

FIGURE 5. $q = 5/2$. Dashed line: initial data. The same initial data is used for both simulations. Solid lines: the solution at various times. Left: $n = 1$; $h_{min}(t)$ occurs at $x = 0$. As t increases, $h_{min}(t)$ decreases and $h_{max}(t)$ increases. At all times there is one minimum per period. Right: $n = 2$. Again, as t increases $h_{min}(t)$ and $h_{max}(t)$ decrease and increase respectively. Initially there is only one local minimum but after some time it splits into two. The minima flank a small 'proto–droplet' and suggest a possible long–time limit of two droplets per period. But, in fact, the proto–droplet drains away as $h_{min} \to 0$.

Our simulations suggest that a second critical exponent, which we call $n_1(q)$, governs the number of local minima per period. If $n < n_1(q)$ then there is one minimum per period. If $n > n_1(q)$ then there are two local minima per period, with their positions moving in time. That is, the single local minimum splits into two as n increases through $n_1(q)$. Goldstein et al. [13, §4C] observed something in a similar spirit for $h_t = -(hh_{xxx})_x - \mathcal{B}(hh_x)_x$, namely a single symmetric singularity that splits into a pair of asymmetric singularities as $\mathcal{B}$ increases past $\mathcal{B} \approx 1.35$.

We find that

$$1 < n_1(5/2) < 1.25.$$

In Figure 6 we plot late–time profiles for a range of n. In the top plot, we plot the solutions near $x = 0$ for $n = 1$ and 1.25. The $n = 1$ profile has only one local minimum, while the $n = 1.25$ profile has two. In the bottom plot, we plot the solutions near $x = 0$ for $n = 1.5$, 1.6 and $n = 1.7$. Each profile has two local minima, with the distance between the minima increasing with n. For each $n \geq 1.25$, we
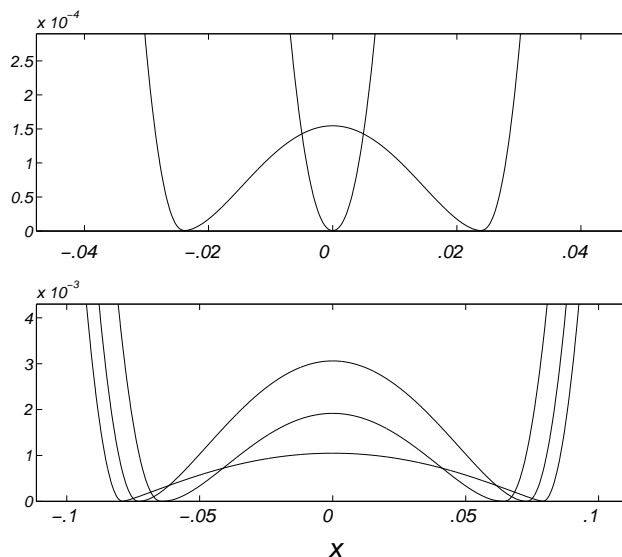
FIGURE 6. $q = 5/2$. Fixed initial data, late–time profiles for the solution of (1.1) computed with different values of n. Top: $n = 1$ (single minimum) and 1.25 (two minima). Bottom: $n = 1.5$, 1.6, 1.7, where the distance between the two minima increases with n.

find that the proto-droplet is draining with its maximum decreasing to zero with a rate that depends on n.

The phrase 'splitting singularities' is perhaps a bit of a misnomer. The two local minima described above do not appear to touch down in a way that yields isolated singularities. Rather, the solution between them appears to be touching down — they are the endpoints of a developing dry interval. A similar phenomenon was observed by Constantin et al. [9, §III,IV] with $n = 1$ and $\mathcal{B} = 0$ (and with different boundary conditions): their proto-droplet decayed like $1/t$.

$\mathbf{q = 1/2}$. For this value of q, we took initial data $h_{ss} - .001h''_{ss}$ and observed phenomena similar to those in the $q = 5/2$ case, finding $1 < n_1(1/2) < 1.25$. We observe behavior similar to that shown in Figure 5 for $q = 5/2$. Specifically, the long–time limit appears to be one droplet. This is interesting since, unlike for $q = 5/2$, if $q = 1/2$ then it is possible to have two disjoint steady droplets in an interval of length 1 (see §A.6.2). And so the proto-droplet could, in theory, converge to a steady droplet. Nonetheless, like for $q = 5/2$, the proto-droplet appears to drain away.

We have not been able to find examples of q, n, and initial data that yield a solution whose long–time limit is a configuration of more than one steady droplet per period.

4. DYNAMICS: q AND ITS EFFECT ON HETEROCLINIC ORBITS

We now consider the evolution equation with a variety of q-values, taking a wide range of initial data near steady states. The resulting solutions display a diversity of behaviors. Our stability theorems [18, 19] often allow us to predict the observed

short–time behavior, and our theorems on the energy levels of steady states [19] often allow us to guess the long–time limit of the solution. As part of this work we predict (and find strong numerical evidence for) heteroclinic connections between certain steady states. Interestingly, there are several cases where we *cannot* predict the long-time behavior of the solution; in particular see the cases $q = 1$ and $3/2$ below.

We present results for seven values of q:

$$q = -3,\ 1/2,\ 1,\ 3/2,\ 1.768,\ 5/2,\ 4,$$

chosen from the intervals $\{(-\infty, -1], (-1, 1), (1, 7/4], (7/4, 1.794), (1.795, 3), [3, \infty)\}$ in which our theorems from [17, 18, 19] suggest the solutions will display distinct behaviors. (How the above intervals were chosen will become clear in what follows. Also, we did study other values of q and found that the phenomena reported here are robust.) For $q = -3$ we take $n = 3$ and $m = -1$. For the other six q-values we take $n = 1$ and $m = q$. Our numerical simulations are not greatly affected if we change n and m in a manner that keeps q fixed, except for the features reported in Section 3.

4.1. $q = -3$: the van der Waals case.
Characteristic features for $q \in (-\infty, -1]$: positive periodic steady states are linearly unstable and there are no droplet steady states with acute contact angles. (See bifurcation diagram 2a and [17, §2.2].) We study the equation

$$h_t = -(h^3 h_{xxx})_x - \mathcal{B}(h^{-1} h_x)_x, \tag{4.1}$$

for which $q = -3$. The equation was proposed by Williams and Davis [28] to model a thin liquid film with net repulsive van der Waals interactions, and more recently it has been studied by Zhang and Lister [31] and by Witelski and Bernoff [29, 30].

4.1.1. $q = -3$. *Perturbing the positive periodic steady state.* First, a positive periodic steady state for $\mathcal{B} = .08930$ is constructed. It is linearly unstable (see Figure 2a). There is at least one linearly unstable eigenfunction for this steady state [18] and hence the unstable manifold is at least one-dimensional. The weakly nonlinear stability analysis suggests that, at least for nearly-constant positive periodic steady states, the unstable manifold is exactly one dimensional.

• *Even perturbations.* The steady state is even and the evolution equation preserves this, after an even perturbation. First we perturb h_{ss} with the even, zero-mean perturbation $\pm \epsilon h''_{\text{ss}}$. Since the perturbation $+\epsilon h''_{\text{ss}}$ lowers the maximum and raises the minimum, one might hope the resulting solution would converge to the constant steady state $h \equiv 1$. If this happens for all small ϵ, then this would be strong evidence for existence of a heteroclinic orbit connecting h_{ss} to the constant steady state.

Perturbing in the direction $+.0001 h''_{\text{ss}}$, we find that after a short transient, the local minimum increases (and maximum decreases) to 1. The extremal points remain fixed in space, while the solution relaxes to the constant steady state as $t \to \infty$; see Figure 7. (This was observed previously in [30, Figure 4b].) We repeated the simulation for smaller values of ϵ and found that all the perturbations yielded solutions that relaxed to the constant steady state as $t \to \infty$. This is convincing evidence that heteroclinic orbits connecting h_{ss} to the constant steady state exist. There are also theoretical reasons to suspect these heteroclinic orbits exist: (i) h_{ss} is energy unstable in the directions $\pm h''_{\text{ss}}$ by [19, Theorem 2], (ii) the energy of h_{ss} is higher than that of the constant steady state $h \equiv 1$ by [19,
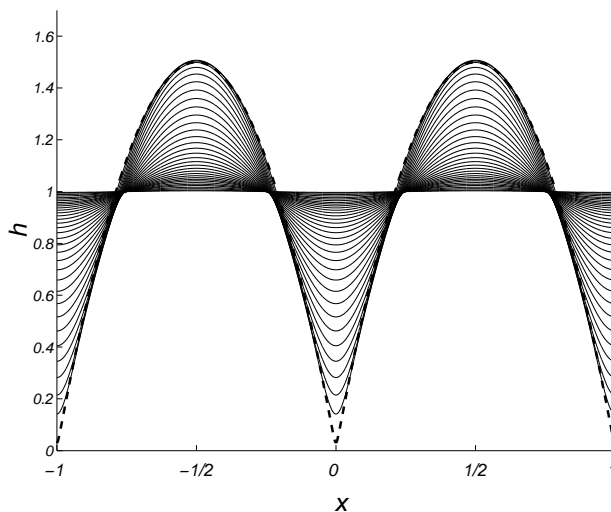
FIGURE 7. $q = -3, n = 3$. Dashed: initial data $h_{\mathrm{ss}} + .0001 h_{\mathrm{ss}}''$. Solid: the solution at a number of times. The local extrema are fixed in space and, after a short transient, h_{min} and h_{max} converge monotonically to 1 and the solution h relaxes to the constant steady state.

Theorem 6] (also observed numerically by Witelski and Bernoff [30, §3]), and (iii) the constant steady state is a local minimum of the energy $\mathcal{E}$ by [19, Theorem 10].

Next we perturb in the opposite direction with $-.0001 h_{\mathrm{ss}}''$, so that the maximum is raised and the minimum lowered. Since the perturbation decreases the energy $\mathcal{E}$, we might expect the solution to subsequently converge to a droplet steady state or to a configuration of droplet steady states. If such a droplet exists it must have $90°$ contact angles, by [17, §2.2]. We find that after a short transient, the minimum height of the solution decreases in time, appearing to decrease to zero in finite time. The top left plot in Figure 8 presents the evolution of the solution near $x = 0$. The local extrema are fixed in space, with the solution appearing to touch down at one point per period. (This was shown previously in [30, Figure 4c].) Computing the derivative h_x of the solution, we find that its maximum and minimum values grow as time passes, as in the bottom left plot of Figure 8. These extremum points of h_x move in time, moving toward $x = 0$ as the singular time approaches. This is consistent with a solution that touches down with $90°$ contact angles in finite time. The right plots in Figure 8 show a late–time profile of h.

The work of Zhang and Lister [31, §5] on similarity solutions suggests that $h(x,t) \sim (t_c - t)^{1/5} H(x/(t_c - t)^{2/5})$ as touchdown approaches; here t_c is the time of touchdown and H is a particular positive function with $H(\eta) \sim (0.807)\, \mathcal{B}^{1/4} |\eta|^{1/2}$ for large η. Our computations are consistent with this ansatz. See [29, 30] for more on the similarity solutions of (4.1).

After the singular time, one possible behavior of the solution shown in Figure 8 is that the solution becomes a nonnegative weak solution. Then it might relax, as a weak solution, to a droplet steady state with $90°$ contact angles. Alternatively, the solution might, at some later time, become positive and classical again, ultimately
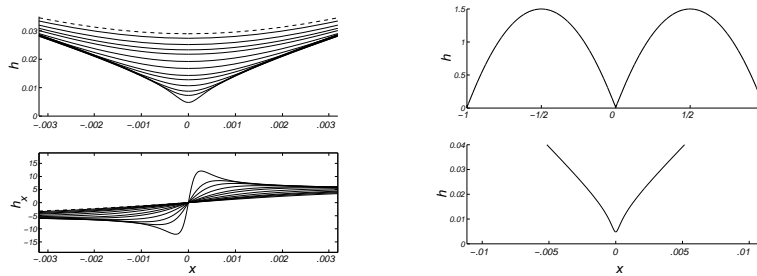
FIGURE 8. Left top: dashed line, initial data $h_{\mathrm{ss}} - .0001h_{\mathrm{ss}}''$; solid lines, solution h at later times. The local minimum is fixed in space and, after a short transient, decrease monotonically to zero. Left bottom: dashed line, initial slope; solid lines, h_x at same times as above. As t passes, $\|h_x\|_\infty$ increases and the positions of the extrema move in toward $x = 0$. This suggests $90°$ contact angles are forming as the singular time approaches. Right top: solution at a late time. Right bottom: a close–up near $x = 0$ at the same time.

relaxing to the constant steady state. This is certainly possible since each profile shown in Figure 8 has higher energy $\mathcal{E}$ than the constant steady state. We note that pursuit of this question will require further analysis, because the current weak existence theory for the evolution equation requires $n \leq m$, whereas here we have $m < n$. Further, the current weak solution theory does not admit $90°$ contact angles unless they occur for a set of times of zero measure. It may be that completely new techniques will have to be developed, to study this equation.

• *Other perturbations.* To check the degree to which the behaviors described above depend on the choice of perturbation, we performed a number of runs with random perturbations. (See §A.7.) We found that all the solutions either relaxed to the constant steady state or else appeared to touch down in finite time. (The gross dynamics are as in Figures 7 and 8; the finer dynamics concern the positions of the local extrema as a function of time.)

4.1.2. $q = -3$. *Perturbing the constant steady state.* Suppose $\mathcal{B} < 4\pi^2$, so that the constant steady state $h \equiv 1$ is linearly stable with respect to zero–mean perturbations of period 1. By [19, Theorem 10], the constant steady state is a strict local minimum of the energy, and is dynamically stable. This is the uninteresting case.

Now suppose $\mathcal{B} > 4\pi^2$. Then the constant steady state $h \equiv 1$ is a saddle point for the diagram 2a), we suspect that a perturbation of the constant steady state will yield a solution that touches down in finite or infinite time.

To investigate, we first take $\mathcal{B} = 2.467 < 4\pi^2$. For all initial data we considered, we found that the resulting solutions appear to relax to the constant steady state. This is as predicted. We then took $\mathcal{B} = 631.7 > 4\pi^2$. Here, the constant steady state has 39 linearly unstable eigenmodes and is a saddle point of the energy. For initial data $1 - .0002\cos(2\pi x)$, the solution appears to touch down in finite time, with one touchdown per period. Figure 9 shows this evolution over two periods.
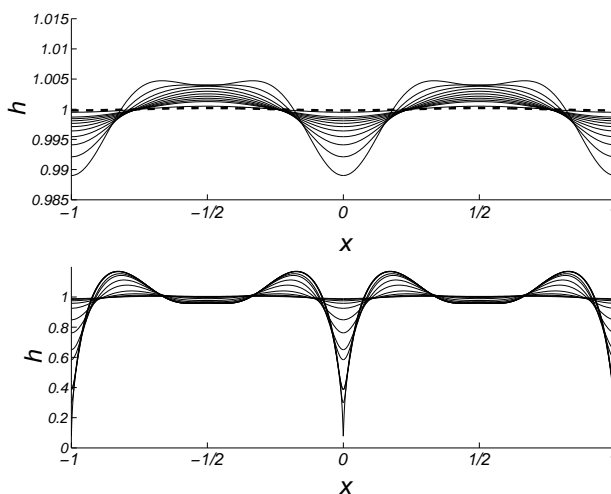
FIGURE 9. $q = -3, n = 3$. Dashed: initial data $1 - .0002 \cos(2\pi x)$. Solid: solution at various times. Top: the short–time dynamics. The local minimum decreases, while the local maximum increases for a while. The top then 'flattens' and two local maxima form one to each side of the flat region. Bottom: later-time dynamics. The solution appears to touch down at one point per period and continues to have two local maxima per period. The local minimum is at $x = 0$ and, after a short transient, decreases monotonically to zero.

Remarks. In our studies of positive periodic steady states and constant steady states, we checked that the observed phenomena persist with smaller perturbations: the behaviors are robust. For this reason, in the remainder of the article we will not discuss smaller perturbations. Further, we will not discuss random perturbations or odd perturbations, since we found that the observed phenomena were like those observed for even perturbations. (Except that for even perturbations the local extrema are fixed in space while for other perturbations they move slightly as the solution evolves.)

We also will not present any further discussions of perturbations of the constant steady state. We found that the behaviors were always those predicted by the bifurcation diagram — if the constant steady state is linearly stable then small perturbations converge back to it, while if the constant steady state is linearly unstable then perturbing it yields a solution that converges to a stable positive periodic steady state, if one exists. If none exists, then we found that the solution either touches down in finite or infinite time ($q < 3$) or else it blows up in finite time ($q \geq 3$).

4.2. **q = 1/2.**

Characteristic features of $q \in (-1, 1)$: positive periodic steady states are linearly unstable. A 'Mountain pass' scenario can occur — the energy of the non-constant positive periodic steady state is higher than the energies of the constant steady state

and the zero-contact angle droplet steady state. (See bifurcation diagram 2b and remarks after [19, Theorem 11].)

We compute solutions of

$$h_t = -(h^1 h_{xxx})_x - \mathcal{B}(h^{1/2}h_x)_x.$$

First, a positive periodic steady state for $\mathcal{B} = 35.59$ is constructed. It is linearly unstable (see Figure 2b). As in §4.1.1, we perturb h_{ss} with $\pm.0001 h''_{\text{ss}}$.

For the initial data $h_{\text{ss}} + .0001 h''_{\text{ss}}$, we see a heteroclinic connection to the constant steady state, very much like in the $q = -3$ case shown in Figure 7.

For the initial data $h_{\text{ss}} - .0001 h''_{\text{ss}}$ we find the solution appears to touch down in finite time. Like the $q = -3$ simulation in Figure 8, $h_{min}(t)$ is located at $x = 0$, and after a short transient the minimum decreases monotonically in time. But unlike the $q = -3$ simulation, the profile seems to touch down with *zero* contact angles. There does exist a zero-angle droplet steady state $\hat{h}_{\text{ss}}$ that has the same area as h_{ss}, has length less than 1, and has lower energy than h_{ss}, by [19, Theorem 7]. Presumably this droplet steady state is the intended long-time limit of the solution, up to translation. But this cannot currently be proved, because the known zero-angle weak existence theory requires $0 < n < 3$ and $q \geq 1$. One might suspect, based on our simulations, that this weak existence theory should be extendable to $q > -1$.

4.3. q = 1.

Characteristic features for $q = 1$: all positive periodic steady states are linearly neutrally stable. (See bifurcation diagram 2c and [19, Lemma 4].)

The non-constant positive periodic steady states are neutrally stable, when $q = 1$. We take $n = m = 1$ and compute solutions of

$$h_t = -(h^1 h_{xxx})_x - \mathcal{B}(h^1 h_x)_x.$$

Numerical simulations for $q = 1$ have been presented before by other authors: with $m = n = 1$ in [13], with $m = n = 2$ in [14, §8], and with $m = n = 3$ in [4]. But the latter two articles do not consider Bond numbers for which periodic steady states might be observed. In the first article, Goldstein et al. [13, Fig. 3a] found that fairly large multi-modal perturbations of positive periodic steady states yield relaxation to (generally different) steady states.

First, we constructed a positive periodic steady state for $\mathcal{B} = 39.48$. In the left plot of Figure 10, we present two simulations confirming that this steady state is dynamically stable, with a small perturbation yielding convergence to a nearby positive periodic steady state. In both cases, the solution relaxes to a positive periodic steady state with a local minimum close to $x = 0$ and an amplitude close to .8. We have no rule for predicting the amplitude of the long–time limit and, unless the perturbation is even, we have no way of predicting the position of the local minimum. The long–time dynamics will be especially difficult to predict when $q = 1$ since there are infinitely many 1-periodic steady states all having area 1. (In the $q \neq 1$ case there are at most two such steady states.)

Since these simulations suggest that the positive periodic steady states are dynamically stable, one might guess that solutions cannot touch down in finite time. (This is what we observe later for $q = 3/2$ and $q = 1.768$.) And as the bottom left plot of Figure 10 suggests, initial data that has a *sharp* local minimum will likely not evolve towards touch–down; the local minimum retracts in time, as expected
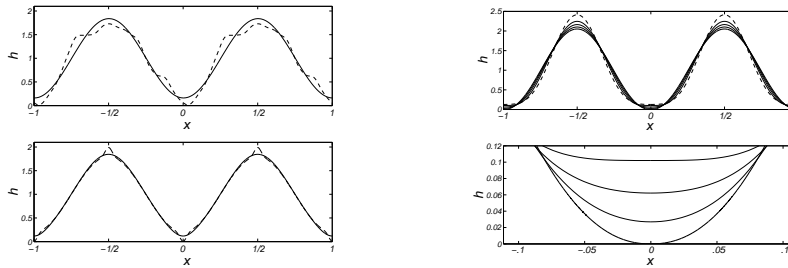
FIGURE 10. $q = 1$, $n = 1$; dashed line: the initial data. Left: the
solid line is a late–time profile of the solution. We found that the
solution relaxes to a steady state close to the original steady state
$1 - .8\cos(2\pi x)$. Top left: $h_0(x) = 1 - .8\cos(2\pi x) + .3v(x)$ where
v is a random zero–mean perturbation. Bottom left: $h_0(x) =
1 - .8\cos(2\pi x) - .19\exp(-100\sin^2(\pi x)) + .19\exp(-100\sin^2(\pi(x -
1/2)))$. Right: $h_0(x) = 1 - 1.143\cos(2\pi x) + .2714\cos(4\pi x)$. Solid
lines are h at various times. The extrema are fixed in space and, af-
ter a short transient, decrease/increase monotonically with $h_{min}(t)$
touching down in finite time.

for a solution of a surface–tension driven flow. On the other hand, initial data that
is very flat near its local minimum does appear to lead to touch–down in finite
time, as shown in the top right plot of Figure 10. The bottom right plot shows this
evolution near the touch–down point.

4.4. q = 3/2.

*Characteristic features for $q \in (1, 7/4]$: positive periodic steady states are linearly
stable.* (See bifurcation diagrams 2d–e.)

We compute solutions of

$$h_t = -(h^1 h_{xxx})_x - \mathcal{B}(h^{3/2}h_x)_x.$$

We constructed a positive periodic steady state h_{ss} for $\mathcal{B} = 40.07$. It is linearly
stable (see Figure 2d).

Also, every perturbation of the same and shorter period increases the energy, by
[19, Theorem 5], and so we expect to observe relaxation back to a translate of h_{ss}.
This is precisely what our simulations show. We have not been able to predict the
amount of translation that occurs, but there is some hope of progress here, since
impressive results on a similar translation problem have been obtained in [7, 8] for
the Cahn–Hilliard equation $h_t = -h_{xxxx} - ((1 - 3h^2)h_x)_x$ on the whole real line.

Next consider zero-mean perturbations of *longer* period, to which h_{ss} is linearly
unstable by [18, Theorem 1]. We ask, to what long-time behavior does this in-
stability give rise? The perturbation $-.0001\cos(\pi x)$, for example, raises the local
minimum of h_{ss} at $x = 1$ and lowers it at $x = 0$. The top plot of Figure 11 presents
the resulting evolution of the 2-periodic solution. The solution appears to touch
down in finite time, though interestingly, it does not do so at $x = 0$. Instead the
touchdown is driven by a dramatic increase in the solution near $x = 1$. The bot-
tom plot of Figure 11 shows a close–up of the final resolved solution. The smaller
droplet, centered on $x = 0$, is not close to a steady droplet since it contains a
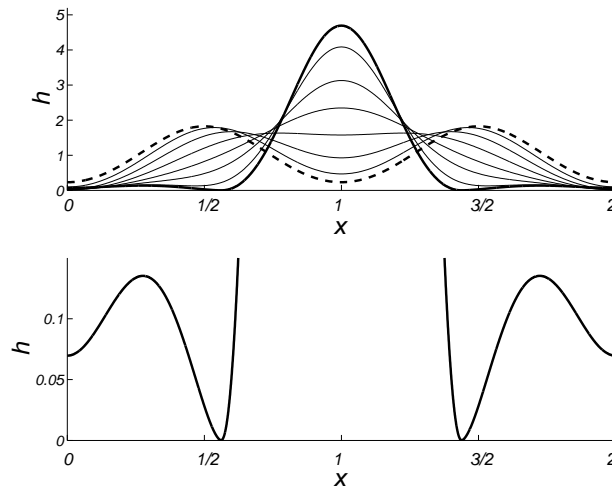
FIGURE 11. $q = 3/2$, $n = 1$. Top plot: dashed line is initial data
$h_{\mathrm{ss}} - .0001\cos(\pi x)$; heavy solid line is final resolved solution; light
solid lines are h at various times. After a short transient, $h(1,t)$
increases monotonically. At late time, a pair of local minima form
to either side of $x = 1$ and touch down in finite time. Bottom plot:
close–up of the final resolved solution.

local minimum within itself — an impossibility for a steady droplet. Therefore
we expect the solution would continue to evolve as a nonnegative weak solution,
relaxing either to a single steady droplet or to some (unknown) configuration of
steady droplets.

4.5. q = 1.768.

*Characteristic features for $q \in (7/4, 1.794)$: some positive periodic steady states
are linearly stable, while others are linearly unstable; and there can be more than
one positive periodic steady state with the same period and area.* (See bifurcation
diagrams 2f–h, and [17, §5.1].)

We compute solutions of

$$h_t = -(h^1 h_{xxx})_x - \mathcal{B}(h^{1.768}h_x)_x.$$

Now the possibility arises of a heteroclinic connection between two fundamentally
different positive periodic steady states. For Bond number $\mathcal{B} = 39.46$ we found
two distinct positive 1-periodic steady states, h_{ss1} and h_{ss2}, that have area 1. We
denote the steady state that has larger amplitude by h_{ss1}, and the other by h_{ss2}. We
expect h_{ss1} to be linearly stable and h_{ss2} to be unstable, by [19, Theorem 9], with
h_{ss1} having lower energy. That is, h_{ss1} lies on the stable branch of the bifurcation
diagram 2g and h_{ss2} lies on the unstable branch. The constant steady state is
linearly stable because $\mathcal{B} < 4\pi^2$.

Our simulations confirmed these predictions. First, all small perturbations of
h_{ss1} resulted in solutions that relaxed back to h_{ss1}. All perturbations of h_{ss2} yielded
solutions that either connect to the constant steady state or to h_{ss1}. Figure 12 shows
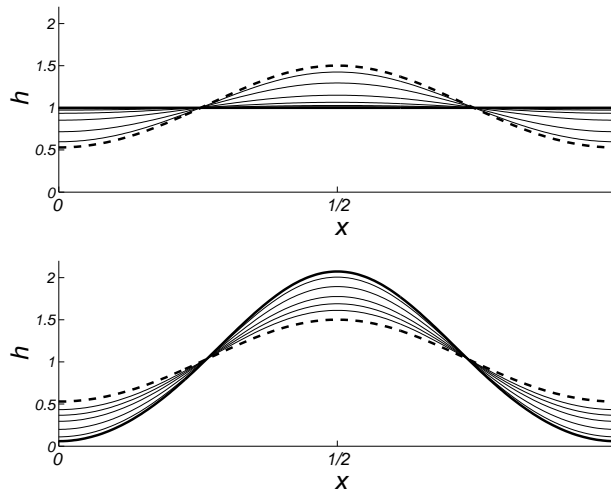a typical pair of solutions.

FIGURE 12. $q = 1.768$ and $n = 1$. The light solid lines are h at a sequence of times. The extrema are fixed in space. (a) Dashed: initial data $h_{\text{ss2}} + .0001h''_{\text{ss2}}$; heavy solid: constant steady state. Solution relaxes to constant. After a short transient, h_{max} and h_{min} converge monotonically to 1 and h relaxes to the constant steady state. (b) Dashed: initial data $h_{\text{ss2}} - .0001h''_{\text{ss2}}$; heavy solid: h_{ss1}. After a short transient, h_{max} increases and h_{min} decreases monotonically, with h relaxing to h_{ss1}.

4.6. **q = 5/2.** *Characteristic features of $q \in (1.795, 3)$: positive periodic steady states are linearly unstable. 'Mountain pass' scenario can occur.* (See bifurcation diagram 2i and remarks after [19, Theorem 11].)

We compute solutions of

$$h_t = -(h^1 h_{xxx})_x - \mathcal{B}(h^{5/2}h_x)_x.$$

We ran one simulation, for $\mathcal{B} = 35.32$, and found behaviors that were qualitatively the same as for $q = 1/2$, in §4.2.

4.7. **q = 4.**

Characteristic features of $q \in [3, \infty)$: positive periodic steady states are linearly unstable, and if a positive periodic steady state and a zero-angle droplet steady state have the same area, then the period of the former is less than the length of the latter. (See [18, Theorem 7] and the proof of [19, Theorem 7].)

We compute solutions of

$$h_t = -(h^1 h_{xxx})_x - \mathcal{B}(h^4 h_x)_x. \tag{4.2}$$

This equation is 'super-critical' in the sense of Bertozzi and Pugh [4], since $m > n+2$ (*i.e.* $q > 3$). According to their conjecture in [4], positive periodic solutions can blow up in finite time, with $\|h(\cdot,t)\|_\infty \to \infty$. Bertozzi and Pugh made the same conjecture for compactly supported weak solutions on the line, and proved in [5] that blow-up can occur in finite time when $n = 1$ and $m \geq n + 2 = 3$. Specifically, they proved for such cases that if the compactly supported initial data h_0 has
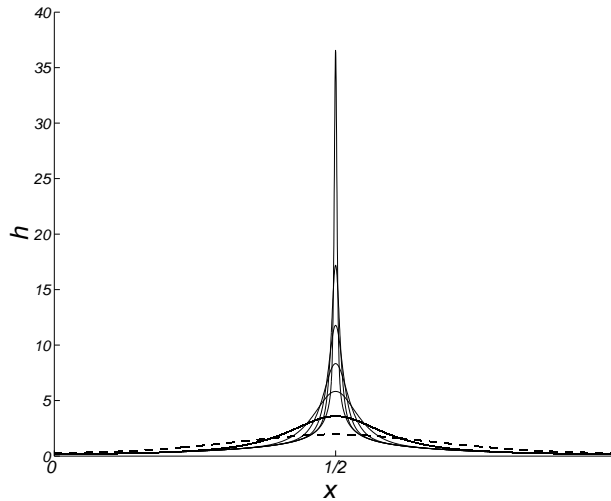
FIGURE 13. $q = 4, n = 1$. Dashed: initial data $h_{\mathrm{ss}} - .001h_{\mathrm{ss}}''$. Solid: h at a sequence of times. The extrema are fixed in space and, after a short transient, h_{max} increases monotonically towards infinity. After a short transient, h_{min} decreases monotonically to a positive value.

negative energy $\mathcal{E}(h_0) < 0$, then the compactly supported weak solution blows up in finite time with its L^∞ and H^1 norms going to infinity.

Here we present computational evidence that positive periodic solutions of (4.2) can also blow up in finite time. Further, we find initial data that has positive energy yet still appears to yield finite–time blow-up, suggesting that $\mathcal{E}(h_0) < 0$ is not necessary for blow-up, in the periodic case.

We took $\mathcal{B} = 22.60$, and found a linearly unstable positive periodic steady state. We considered initial data $h_{\mathrm{ss}} \pm .001h_{\mathrm{ss}}''$. The initial data $h_{\mathrm{ss}} + .001h_{\mathrm{ss}}''$ yielded a solution that relaxed to the constant steady state.

The initial data $h_{\mathrm{ss}} - .001h_{\mathrm{ss}}''$ yielded a solution that appears to blow up in finite time (see Figure 13). A self-similarity ansatz suggests that $h(x,t) \sim (t_c - t)^{-1/7}H((x-1/2)/(t_c - t)^{3/14})$ as blowup approaches. Here t_c is the time of blowup and H is a positive function with $H(\eta) \sim C|\eta|^{-2/3}$ for large η. Our simulations are consistent with this ansatz. Self–similar blow-up for super-critical exponents has also been found for $h_t = -(h^3 h_{xxx})_x - \mathcal{B}(h^6 h_x)_x$ (presented by Bertozzi and Pugh at the APS Division of Fluid Dynamics meeting, November 1997).

5. Conclusions and Future Directions

We have numerically studied the evolution equation $h_t = -(h^n h_{xxx})_x - \mathcal{B}(h^m h_x)_x$. Our work suggests that the energy landscape through which solutions travel is fairly simple and that understanding the relative energy levels of the steady states gives considerable insight into the dynamics of the solutions. In particular we have found strong evidence for the existence of heteroclinic connections between steady states,

connections we conjecture to exist based on our theorems [19] on the relative energy levels of steady states. It is an open problem to prove analytically that these connections exist.

In §3 we presented numerical results on the persistence of heteroclinic connections under changes in the mobility parameters n and m. We changed n and m in a way that preserved $q = m - n + 1$, preserving the energy $\mathcal{E}$ and hence the steady states and energy landscape. But the timescale of the dynamic solution did change noticeably in response to changes in the mobilities, even though the shape of the solution changed little.

We would expect these structural stability observations to continue to hold if the mobilities were changed in a way that, while not fixing q, perturbed it only a little (so that the energy landscape is also perturbed only a little).

In §3 we further investigated critical mobility exponents, such as the critical n above which solutions remain positive for all time (in other words, the critical exponent for film rupture or pinch-off). An interesting question for the future is to find formulas for the critical mobility exponents. These critical exponents determine important qualitative features of the evolution, and determining them would shed considerable light not only on the equation studied here but also on related equations that arise from physical models.

Lastly, in §4 we demonstrated that the physical quantities P, A, $\mathcal{B}$, and $m - n$ appear to fully determine the large-scale features of the evolution, since they determine the steady states and the energy landscape via the bifurcation parameter $E = \mathcal{B}A^{q-1}P^{3-q}$. Finer details, such as the motion of the extrema in time, depend on the initial data. Also, we have not been able to predict the amount of translation of a solution that might occur in the long-time limit.

Another open problem is to determine precisely the long-time limit of an evolution that approaches a steady droplet configuration. In part the difficulty is that translates of steady droplets are also steady droplets, so that even if one knows the length and area of each droplet in the configuration, their locations relative to each other must still be determined. Thus droplet attractors might have rather high dimension.

In conclusion, we hope our numerical investigations of the power law evolution (1.1) will provide resources, ideas and motivation for researchers studying $h_t = -(f(h)h_{xxx})_x - (g(h)h_x)_x$ with non-power law coefficient functions f and g. Some such numerical studies exist already. For example, the papers [14, 23] consider an f that is degenerate ($f(0) = 0$) and g's that are not power laws, and there is of course a large literature on the (non-degenerate) Cahn–Hilliard equation.

the James Franck Institute of the University of Chicago. M. Pugh thanks Todd Dupont and Bastiaan Braams for illuminating conversations regarding numerical issues.

APPENDIX A. NUMERICAL METHODS AND PARAMETERS USED IN SIMULATIONS

The numerical simulations are done using a finite-difference evolution code. Throughout this section the exponent ℓ denotes the ℓth time-step and h^ℓ is the numerical approximation of the solution at time $t_\ell = \ell \Delta t$. The diffusion coefficients are represented as functions f and g.

A.1. **The evolution code.** We use an adaptive time–stepping scheme (discussed in §A.3) based on a Crank-Nicolson scheme:

$$
\begin{aligned}
\frac{h^{\ell+1} - h^\ell}{\Delta t} \;=\; & -\frac{1}{2}\left(f(h^{\ell+1/2})h^{\ell+1}_{xxx}\right)_x - \frac{1}{2}\left(f(h^{\ell+1/2})h^\ell_{xxx}\right)_x \\
& -\frac{1}{2}\left(g(h^{\ell+1/2})h^{\ell+1}_x\right)_x - \frac{1}{2}\left(g(h^{\ell+1/2})h^\ell_x\right)_x .
\end{aligned}
$$

The diffusion coefficients are evaluated at $h^{\ell+1/2}$, which we find by linearly extrapolating the solutions $h^{\ell-1}$ and h^ℓ to time $t_\ell + \Delta t/2$. The local truncation error is $O(\Delta t^3)$ in time intervals where Δt is fixed and is $O(\Delta t^2)$ at times when the timestep is changed.

Finding $h^{\ell+1}$ reduces to solving a linear problem, which we write in a residual formulation:

$$
\mathcal{L}z = -\Delta t \left[f(h^{\ell+1/2})(h^\ell_{xxx} + r(h^{\ell+1/2})h^\ell_x) \right]_x \tag{A.1}
$$

where $z = h^{\ell+1} - h^\ell$, $r(y) = g(y)/f(y)$, and the linear operator $\mathcal{L}$ is

$$
\mathcal{L}z := z + \Delta t\, \frac{1}{2}\left[f(h^{\ell+1/2})(z_{xxx} + r(h^{\ell+1/2})z_x) \right]_x .
$$

The scheme uses $h^{\ell-1}$ and h^ℓ to compute $h^{\ell+1}$; for the first step we take $h^{-1} = h^0$.

Performing a linear stability analysis about a constant steady state, we find the scheme is stable. Specifically, perturbations whose wave numbers are outside the unstable band of the linearized PDE do not grow.

For the spatial discretization, the key issue is to implement the scheme in a way that preserves steady states. A steady state h_{ss} satisfies $(h_{\text{ss}})_{xxx} + r(h_{\text{ss}})(h_{\text{ss}})_x = 0$ [25, 17]. Such an 'analytic steady state' will be $O(\Delta x^2)$-close to the 'finite-difference' steady state $\tilde{h}$ satisfying the following discretization:

$$
\tilde{h}_{i+2} - 3\tilde{h}_{i+1} + 3\tilde{h}_i - \tilde{h}_{i-1} + \Delta x^2 \frac{r(\tilde{h}_{i+1}) + r(\tilde{h}_i)}{2}\left(\tilde{h}_{i+1} - \tilde{h}_i\right) = 0, \quad i = 1 \dots N. \tag{A.2}
$$

The meshpoints are $x_1 = \Delta x, x_2 = 2\Delta x, \cdots, x_N = P$, where P is the length of the interval, and we denote the function values at the meshpoints with subscripts: $\tilde{h}_1, \tilde{h}_2, \dots \tilde{h}_N$. The function is periodic: $\tilde{h}_0 = \tilde{h}_N$.

To implement the residual formulation (A.1), we apply the $O(\Delta x^2)$ approximation

$$
\begin{aligned}
\left[(f(h)(z_{xxx} + r(h)z_x))_x\right]_i \;\simeq\; & \frac{f_{i+}}{\Delta x}\left(\frac{z_{i+2} - 3z_{i+1} + 3z_i - z_{i-1}}{\Delta x^3} + r_{i+}\frac{z_{i+1} - z_i}{\Delta x} \right) \\
& -\frac{f_{i-}}{\Delta x}\left(\frac{z_{i+1} - 3z_i + 3z_{i-1} - z_{i-2}}{\Delta x^3} + r_{i-}\frac{z_i - z_{i-1}}{\Delta x} \right) \tag{A.3}
\end{aligned}
$$

where the subscripts $i+$ and $i-$ denote the right-average and left-average:

$$r_{i+} := \frac{r(h_{i+1}) + r(h_i)}{2}, \qquad r_{i-} := \frac{r(h_i) + r(h_{i-1})}{2}.$$

This approximation yields a $O(\Delta x^2)$-accurate $N \times N$ matrix approximation $\tilde{\mathcal{L}}$ of the operator $\mathcal{L}$:

$$\tilde{\mathcal{L}}\vec{z} = R\vec{H}S(h^{\ell-1}, h^\ell).$$

$\tilde{\mathcal{L}}$ is pentadiagonal periodic. The righthand side of (A.1) is discretized analogously.

It follows immediately from (A.2) that the time-stepping scheme preserves finite-difference steady states. Also, by factoring f out we have also isolated the pressure gradient term in the equation, $(h_{xx} + \mathcal{B}/q\, h^q)_x$.

A.2. **Computing the finite-difference steady state.** Here, we only discuss the case of power law coefficients $f(h) = h^n$ and $g(h) = \mathcal{B}h^m$. Given N uniformly distributed meshpoints between 0 and $P = 1$, we seek a finite-difference steady state $\tilde{h}$ that solves the N equations (A.2) to the level of round-off error. We do this with Newton–Raphson iteration. To do this, we need a good first guess for $\tilde{h}$. In the following, we describe how we find a first guess and then how we execute the iteration.

Given the exponent $q \neq 0$ we first compute the rescaled steady state $k = k_\alpha$ at the N points $x = P/N, 2P/N, \cdots, P$. As described in [17, §6.1], we do this by viewing the steady state equation

$$k_{xx} + \frac{k^q - 1}{q} = 0, \qquad k(0) = \alpha, \quad k_x(0) = 0, \tag{A.4}$$

as an initial value problem in x. We verify that k is spectrally accurate by using a discrete fast Fourier transform to check that the power-spectrum is fully resolved (cf. §A.5). For numerical purposes, k is an exact solution of equation (A.4), and so in the following we refer to it as an 'analytic steady state'.

Once the analytic steady state k is known, we rescale it to find an analytic steady state h_{ss} of period 1 and area 1. Specifically, if P and A are the period and area of k, then we use the rescalings [17, (3.3),(5.1)] to determine

$$\mathcal{B} = A^{q-1}P^{3-q} \quad \text{and} \quad h_{\text{ss}} = \frac{P}{A}k.$$

We note that k, and hence $A = A(\alpha)$ and $P = P(\alpha)$, are determined by the initial value α in (A.4). Varying α, one finds a family of 1-periodic steady states of area 1 each with a different amplitude and satisfying the steady state equation with a different value of $\mathcal{B}$. This was used in constructing the bifurcation diagrams in Figure 2.

To find the finite-difference steady state $\tilde{h}$ close to h_{ss} we need to solve the N equations (A.2), which we write as

$$\vec{F}(\tilde{h}) := M\tilde{h} + \vec{V}(\tilde{h}) = \vec{0}$$

where M is a tetradiagonal periodic matrix and $\vec{V}(\tilde{h})_i$ is a nonlinear function of $\tilde{h}_i$ and $\tilde{h}_{i+1}$. The Newton–Raphson iteration is

$$\tilde{h}^{new} = \tilde{h}^{old} - (D\vec{F}(\tilde{h}^{old}))^{-1}\vec{F}(\tilde{h}^{old}).$$

To iterate, one has to solve $D\vec{F}\vec{x} = \vec{F}(\tilde{h}^{old})$. We find that $D\vec{F}$ is a singular matrix of rank $N - 1$. We solve $D\vec{F}\vec{x} = \vec{F}(\tilde{h}^{old})$, using the singular value decomposition

of $D\vec{F}$ obtained using LAPACK's 'dgesvd.f' to solve for $\vec{x}$. The iteration is then started with the initial guess h_{ss} and stopped when the largest error in the N equations (A.2) is less than 10^{-14}.

Note: For $q = 1$, the finite–difference steady states satisfy a linear problem:

$$\tilde{h}_{i+2} - 3\tilde{h}_{i+1} + 3\tilde{h}_i - \tilde{h}_{i-1} + \Delta x^2 \tilde{\mathcal{B}}\left(\tilde{h}_{i+1} - \tilde{h}_i\right) = 0, \quad i = 1 \dots N.$$

Analytic steady states are $a + b\cos(\sqrt{\mathcal{B}}x + \phi)$ and are 1-periodic if $\sqrt{\mathcal{B}}$ is $n2\pi$ for some integer n. Sampling such a steady state on a uniform mesh gives

$$\tilde{h}_j = a + b\cos(\sqrt{\mathcal{B}}\,j\Delta x + \phi),$$

and one can check that $\tilde{h}$ is a finite–difference steady state provided

$$\tilde{\mathcal{B}} = 2\,\frac{1 - \cos(\sqrt{\mathcal{B}}\Delta x)}{\Delta x^2} = \mathcal{B} - O(\Delta x^2).$$

That is, there are nontrivial analytic steady states for a countable collection of Bond numbers, $\sqrt{\mathcal{B}} \in \{2\pi, 4\pi, 6\pi, \dots\}$, and nontrivial finite difference steady states for a nearby countable set of Bond numbers $\tilde{\mathcal{B}}$.

A.3. **Timestepping and accuracy.** The adaptive timestepping controls the accuracy as follows. An error tolerance is set, $\epsilon = 10^{-11}$. At each time step, we first use the Crank-Nicolson scheme to compute h_1, an approximation of the solution at time $t + \Delta t$. We then take two timesteps with $\Delta t/2$ to compute h_2, another approximation of the solution at time $t + \Delta t$. For some constant C, the error is bounded [16, §5.2] by the difference of h_1 and h_2:

$$\|h(\cdot, t + \Delta t) - h_2\|_\infty \le C\|h_1 - h_2\|_\infty.$$

If $\|h_1 - h_2\|_\infty > \epsilon$ then we replace Δt with $\Delta t/2$ and try again (without advancing in time). If $\|h_1 - h_2\|_\infty < \epsilon/10$ then we replace Δt with $2\Delta t$ and try again. If $\|h_1 - h_2\|_\infty$ lies between ϵ and $\epsilon/10$ then we just take the solution at time $t + \Delta t$ to be h_2. Admittedly, since we do not know the constant C this error control is valid only as long as C is not large.

In practice, we find that the timestep is initially reduced to resolve the initial fast transient and then coarsens. After this, the timestep is rarely reduced, except near times when the run has to be stopped anyway in order to point–double to resolve the growing derivatives of the solution.

A.4. **Stopping criteria and issues for singularities.** To test whether to stop the code, we compute the minimum value of h^ℓ at each time-step. If this minimum is less than or equal to zero, then we stop the code. This is a natural stopping criterion since for any equation in flux form $h_t + (hU)_x = 0$, if $h_{min}(t) \downarrow 0$ then $U_x \to \infty$ at the location of h_{min}. Because U is determined by h and its derivatives, this blow-up signals a loss of smoothness in h.

Stopping of the code thus suggests a finite-time singularity, but we emphasize that the code was designed to preserve the periodic steady states and not to carefully resolve singularities. Hence in reality the singularity may occur in infinite time, with the stopping criterion being met in finite time because of oscillations in the profile (possibly caused by loss of spectral resolution). Also, since the code has no local mesh refinement, we have to over-resolve much of the solution in order to resolve it near the singular points, where it is tending to zero. This over–resolution slows

the computation significantly. To examine fine details of the temporal and spatial scales of the singularities, then, one should implement a code that has an adaptive spatial mesh.

If a smooth solution touches down in finite time, it may continue to evolve as a weak solution. Weak solutions also arise when the initial data has compact support; the degeneracy of the equation can provide finite-speed of propagation of the support. Computing the evolution of weak solutions is truly nontrivial. We refer interested readers to [1, 15, 32].

A.5. **Point-doubling and keeping solutions spectrally resolved.** In §4.1.1, we present a simulation with initial data $h_{\rm ss} - .0001 h_{\rm ss}''$ for the evolution equation with $q = -3$ and $n = 3$. There, we find that the solution appears to touch-down in finite time. As the minimum height decreases, the curvature increases, requiring that after some time the number of meshpoints be increased to keep the solution spectrally resolved. We do this as follows. We compute the solution with 2,048 meshpoints until the computation stops because positivity is lost. We look at the power spectrum of the solution and choose a time right before the active part of the power-spectrum is reaching the Nyquist frequency. That is, we find the last time at which the 1,023rd Fourier amplitude of the solution is at the level of round–off. We take the solution at this time and compute its Fourier coefficients, defined for wave numbers $-{\rm N}/2 + 1 \leq k \leq {\rm N}/2 - 1$ where ${\rm N} = 2,048$. We pad by zeros, extending the Fourier coefficients to be defined for wave numbers $-{\rm N} + 1 \leq k \leq {\rm N} - 1$, and then compute the inverse Fourier transform. This yields a function on 2N meshpoints that is indistinguishable from the solution at that time, to the level of round–off. Using this function as initial data, we continue the computation on 2N meshpoints, repeating this point–doubling process whenever the solution becomes unresolved.

A.6. **The simulations of Sections 3 and 4.**

A.6.1. *Notes on the $q = 5/2$ simulations in §3.* We computed a 1-periodic steady state $h_{\rm ss}$ on 256 meshpoints with Bond number $\mathcal{B} = 35.32$ and area 1, by rescaling k_α with $\alpha = 0.2145$, $P = 6.869$, and $A = 5.663$. All of the simulations shown in Figures 4-5 were run until the 8,192 meshpoint simulation lost resolution, except for the $n = 1.6625$ simulation which required 65,536 meshpoints to resolve the solution when h_{min} was at its smallest. All the profiles shown in Figure 6 are the final resolved solution with 8,192 meshpoints.

We now prove our earlier claim that for $q = 5/2$ and $\mathcal{B} = 35.32$, there cannot be two disjoint zero contact angle steady droplets in an interval of length 1, if the total area of the droplets is 1. There does exist a *single* zero angle droplet steady state with that area and with length less than 1 — its length is $P = (E_0(5/2)/\mathcal{B})^2 = .8414 < 1$, where $E_0(5/2) = 32.40$ by [17, §3.1.2]. Hence there is a zero contact angle droplet to which the solution on the right of Figure 5 could relax. But if there were a pair of zero contact angle steady state droplets, with areas $A_1 = \lambda$ and $A_2 = (1 - \lambda)$, then the combined length of the two droplets would be

$$P_1 + P_2 = \left(\lambda^{-3} + (1 - \lambda)^{-3}\right)(E_0(5/2)/\mathcal{B})^2.$$

The righthand side is a convex function of λ, achieving its minimum value 13.46 at $\lambda = 1/2$. This minimum value is greater than 1, and so one cannot fit the two droplet steady states in an interval of length 1. Thus the simulations described

earlier cannot be converging to a pair of steady zero contact angle droplets. Indeed, our computations show the proto-droplet is slowly draining.

A.6.2. *Notes on the $q = 1/2$ simulations in §3.* We computed a 1-periodic steady state h_{ss} on 256 meshpoints with Bond number $\mathcal{B} = 36.29$ and area 1, by rescaling k_α with $\alpha = 0.2145$, $P = 6.168$, and $A = 6.779$.

We now prove our earlier claim that for $q = 1/2$ and $\mathcal{B} = 36.29$ there can be two disjoint zero contact–angle droplets in an interval of length 1, if their total area is 1. A single zero contact angle steady state would satisfy [17, §3.1.2]

$$ P = A^{1/5} \left(E_0(1/2)/\mathcal{B} \right)^{2/5}, \qquad \text{with } A = 1 $$

where $E_0(.5) = 32.86$. We find $P = .9611 < 1$. Thus a single zero contact angle steady state is a potential long–time limit. For two zero contact angle steady states, we find

$$ P_1 + P_2 = \left(\lambda^{1/5} + (1 - \lambda)^{1/5} \right) \left(E_0(1/2)/\mathcal{B} \right)^{2/5}. $$

This is a concave function with its maximum at $\lambda = 1/2$. We find that $P_1 + P_2 < 1$ if $\lambda \leq 10^{-7}$ (approx.) and so one *can* have two zero contact angle droplets — but one of them must be fairly small. For example, if $\lambda = 10^{-7}$ then the length of the smaller droplet is $P_1 = 0.03826$. In our $n = 2$ simulation, the distance between the local minima was .03869 when we stopped the code. This is close to .02826; thus a two–droplet long–time limit is at least a possibility.

A.6.3. *Notes on the $q = -3$ simulations in §4.1.1.* We computed a 1-periodic steady state h_{ss} on 2048 meshpoints with Bond number $\mathcal{B} = .08930$ and area 1, by rescaling k_α with $\alpha = 0.2145$, $P = 16.32$, and $A = 120.6$. The steady state h_{ss} has large curvature at its local minima, and so we need a large number of meshpoints to resolve the initial data $h_{ss} + .0001h''_{ss}$ with spectral accuracy. We find that for a solution on $[0, 1)$ we need 2,048 meshpoints (following §A.5). For the initial data $h_{ss} - .0001h''_{ss}$, the resulting solution appears to touch down in finite time, requiring point–doubling as the solution's curvature increases (see §A.5.) In this way, we computed a resolved solution to time $t = 56.0019$ at which time the 32,768 meshpoint solution became spectrally unresolved. For the simulation with initial data $1 - .0002\cos(2\pi x)$ we started with 256 meshpoints and stopped at time $t = 31050.2$ with 16,384 meshpoints.

A.6.4. *Notes on the $q = .5$ simulations in §4.2.* We computed a 1-periodic steady state h_{ss} on 512 meshpoints with Bond number $\mathcal{B} = 33.73$ and area 1, by rescaling k_α with $\alpha = 0.03000$, $P = 6.049$, and $A = 7.122$. The simulation with initial data $h_{ss} - .0001h''_{ss}$ stopped at $t = 9525.89$ with 8,192 meshpoints.

A.6.5. *Notes on the $q = 1$ simulations in §4.3.* We found a 256-meshpoint finite–difference steady state for $\mathcal{B} \sim 4\pi^2$ (see §A.2). We used perturbations of this steady state for all three simulations in Figure 10. The simulation in Figure 10b stopped at time $t = 1320.07$, with 32,768 meshpoints.

A.6.6. *Notes on the $q = 3/2$ simulations in §4.4.* We computed a 1-periodic steady state h_{ss} on 256 meshpoints with Bond number $\mathcal{B} = 40.07$ and area 1, by rescaling k_α with $\alpha = 0.2145$, $P = 6.453$, and $A = 5.975$. The simulation with initial data $h_{ss} - .0001\cos(x/2)$ stopped at $t = 109594$ with 4,096 meshpoints.

A.6.7. *Notes on the $q = 1.768$ simulations in §4.5.* We now explain how we found the two steady states h_{ss1} and h_{ss2} having period 1 and area 1 that are both steady states for $\mathcal{B} = 39.46$. Let $E(\alpha) = A(\alpha)^{q-1}P(\alpha)^{3-q}$. First we plot $E(\alpha)$ for $\alpha \in (0,1)$. We seek $\alpha_1 < \alpha_2$ such that $E(\alpha_1) = E(\alpha_2)$ with $E'(\alpha_1) < 0$ and $E'(\alpha_2) > 0$. Choosing $\alpha_1 = .05$, we find that the desired α_2 exists (see [19, Figure 5]). To determine α_2, we first compute k_{α_1} and find its period $P(\alpha_1) = 6.703$, area $A(\alpha_1) = 5.660$, and $E(\alpha_1) = 39.46$. From the graph of $E(\alpha)$, we make a rough estimate of α_2 and choose six values of α such that $E(\alpha) < E(\alpha_2) = E(\alpha_1)$ at the first three values and $E(\alpha) > E(\alpha_2)$ at the last three values: then α_2 is between the third and fourth values. We interpolate E at the six values of α with a quintic polynomial and use Newton–Raphson iteration to find $\alpha_2 = 0.5069$ satisfying $E(\alpha_1) = E(\alpha_2)$. We find k_{α_2} has period $P(\alpha_2) = 6.388$ and area $A(\alpha_2) = 6.115$. We then rescale k_{α_1} to h_{ss1} and k_{α_2} to h_{ss2}. By construction, they are distinct positive periodic steady states for $\mathcal{B} = 39.46$. All of the simulations were done with 256 meshpoints.

A.6.8. *Notes on the $q = 5/2$ simulations in §4.6.* We computed a 1-periodic steady state h_{ss} on 256 meshpoints with Bond number $\mathcal{B} = 35.32$ and area 1, by rescaling k_α with $\alpha = 0.2145$, $P = 6.869$, and $A = 5.663$. The simulation with initial data $h_{ss} - .0001h_{ss}''$ stopped at $t = 101368$ with 2,048 meshpoints.

A.6.9. *Notes on the $q = 4$ simulations in §4.7.* We computed a 1-periodic steady state h_{ss} on 256 meshpoints with Bond number $\mathcal{B} = 22.60$ and area 1, by rescaling k_α with $\alpha = 0.2145$, $P = 7.536$, and $A = 5.543$. The energy $\mathcal{E}(h_0) = .3471$ is positive. The simulation with initial data $h_{ss} - .001h_{ss}''$ stopped $t = 30565.4$ with 4,096 meshpoints. At that time, h_{max} had increased by a factor of 36.57.

A.7. **Finding random perturbations.** A function on 2,048 meshpoints can resolve 1,023 frequencies, so we choose $\{a_k\}$ and $\{\phi_k\}$ to be two sets of 1,023 uniformly distributed random numbers in $[0,1]$ and define the perturbation

$$\phi(x) = \sum_{k=1}^{1,023} a_k \exp(-.036k) \cos(k2\pi x + \phi_k).$$

This perturbation has zero mean, and has random amplitudes and phases at each wave–number. The decay rate 0.036 is chosen so that the amplitudes at wave numbers $k = 900$ and higher are at the level of round–off error, meaning the initial data is spectrally resolved. We then normalized ϕ to have L^∞ norm equal to 1. (In fact, we normalized all perturbations in the article in this way.) Random perturbations on other mesh-sizes are constructed analogously.

References

[1] J. W. Barrett, J. F. Blowey, and H. Garcke. Finite element approximation of a fourth order nonlinear degenerate parabolic equation. *Numer Math*, 80(4):525–556, 1998.

[2] A. J. Bernoff, A. L. Bertozzi, and T. P. Witelski. Axisymmetric surface diffusion: dynamics and stability of self-similar pinchoff. *J. Statist. Phys.*, 93(3-4):725–776, 1998.

[3] A. L. Bertozzi, M. P. Brenner, T. F. Dupont, and L. P. Kadanoff. Singularities and similarities in interface flow. In L. Sirovich, editor, *Trends and Perspectives in Applied Mathematics*, volume 100 of *Applied Mathematical Sciences*, pages 155–208. Springer–Verlag, New York, 1994.

[4] A. L. Bertozzi and M. C. Pugh. Long–wave instabilities and saturation in thin film equations. *Commun Pur Appl Math*, 51:625–661, 1998.

[5] A. L. Bertozzi and M. C. Pugh. Finite-time blow-up of solutions of some long-wave unstable thin film equations. *Indiana Univ. Math. J.*, 49(4):1323–1366, 2000.

[6] Wolf-Jürgen Beyn, Alan Champneys, Eusebius Doedel, Willy Govaerts, Yuri A. Kuznetsov, and Björn Sandstede. Numerical continuation, and computation of normal forms. In *Handbook of dynamical systems, Vol. 2*, pages 149–219. North-Holland, Amsterdam, 2002.

[7] J. Bricmont, A. Kupiainen, and J. Taskinen. Stability of Cahn-Hilliard fronts. *Commun Pur Appl Math*, 52(7):839–871, 1999.

[8] E. A. Carlen, M. C. Carvalho, and E. Orlandi. A simple proof of stability of fronts for the Cahn-Hilliard equation. *Commun. Math. Phys.*, 224(1):323–340, 2001.

[9] P. Constantin, T. F. Dupont, R. E. Goldstein, L. P. Kadanoff, M. J. Shelley, and S.-M. Zhou. Droplet breakup in a model of the Hele–Shaw cell. *Phys Rev E*, 47(6):4169–4181, June 1993.

[10] E. J. Doedel, M. J. Friedman, and B. I. Kunin. Successive continuation for locating connecting orbits. *Numer. Algorithms*, 14(1-3):103–124, 1997. Dynamical numerical analysis (Atlanta, GA, 1995).

[11] Paul C. Fife. Models for phase separation and their mathematics. *Electron. J. Differential Equations*, pages No. 48, 26 pp. (electronic), 2000. Originally written in June 1991.

[12] Paul C. Fife. Pattern formation in gradient systems. In *Handbook of dynamical systems, Vol. 2*, pages 677–722. North-Holland, Amsterdam, 2002.

[13] R. Goldstein, A. Pesci, and M. Shelley. Instabilities and singularities in Hele–Shaw flow. *Phys Fluids*, 10(11):2701–2723, 1998.

[14] G. Grün and M. Rumpf. Simulation of singularities and instabilities arising in thin film flow. *Eur J Appl Math*, 12(3) 3:293–320, 2001.

[15] Günther Grün and Martin Rumpf. Nonnegativity preserving convergent schemes for the thin film equation. *Numer. Math.*, 87(1):113–152, 2000.

[16] A. Iserles. *A first course in the numerical analysis of differential equations*. Cambridge University Press, Cambridge, 1996.

[17] R. S. Laugesen and M. C. Pugh. Properties of steady states for thin film equations. *Eur J Appl Math*, 11(3):293–351, 2000.

[18] R. S. Laugesen and M. C. Pugh. Linear stability of steady states for thin film and Cahn–Hilliard type equations. *Arch Ration Mech An*, 154(1):3–51, 2000.

[19] R. S. Laugesen and M. C. Pugh. Energy levels of steady states for thin film type equations. *J Diff Eq*, 182(2):377–415, 2002.

[20] G. J. Lord, A. R. Champneys, and G. W. Hunt. Computation of homoclinic orbits in partial differential equations: an application to cylindrical shell buckling. *SIAM J. Sci. Comput.*, 21(2):591–619 (electronic), 1999.

[21] P. Manneville. *Dissipative structures and weak turbulence*. Academic Press Inc., Boston, MA, 1990.

[22] T. G. Myers. Thin films with high surface tension. *SIAM Rev.*, 40(3):441–462 (electronic), 1998.

[23] A. Oron and S. G. Bankoff. Dewetting of a heated surface by an evaporating liquid film under conjoining/disjoining pressures. *J Colloid Interface Sci*, 218(1):152–166, 1999.

[24] A. Oron, S. H. Davis, and S. G. Bankoff. Long–scale evolution of thin liquid films. *Rev Mod Phys*, 69(3):931–980, Dec 1997.

[25] A. Oron and P. Rosenau. Formation of patterns induced by thermocapillarity and gravity. *J Phys II*, 2:131–146, 1992.

[26] F. Otto. Lubrication approximation with prescribed non–zero contact angle: an existence result. *Commun Part Diff Eq*, 23:2077–2164, 1998.

[27] J. E. Taylor and J. W. Cahn. Linking anisotropic sharp and diffuse surface motion laws via gradient flows. *J. Statist. Phys.*, 77(1-2):183–197, 1994.

[28] M. B. Williams and S. H. Davis. Nonlinear theory of film rupture. *J Colloid Interf Sci*, 90(1):220–228, 1982.

[29] Thomas P. Witelski and Andrew J. Bernoff. Stability of self-similar solutions for van der Waals driven thin film rupture. *Phys. Fluids*, 11(9):2443–2445, 1999.

[30] Thomas P. Witelski and Andrew J. Bernoff. Dynamics of three-dimensional thin film rupture. *Phys. D*, 147(1-2):155–176, 2000.

[31] W. W. Zhang and J. R. Lister. Similarity solutions for van der Waals rupture of a thin film on a solid substrate. *Phys Fluids*, 11(9):2454–2462, 1999.

[32] L. Zhornitskaya and A. L. Bertozzi. Positivity-preserving numerical schemes for lubrication-type equations. *SIAM J. Numer. Anal.*, 37(2):523–555 (electronic), 2000.

RICHARD. S. LAUGESEN

DEPARTMENT OF MATHEMATICS, UNIVERSITY OF ILLINOIS, URBANA, IL 61801, USA
　E-mail address: laugesen@math.uiuc.edu

MARY C. PUGH

DEPARTMENT OF MATHEMATICS, UNIVERSITY OF TORONTO, TORONTO, ON M5S 3G3, CANADA
　E-mail address: mpugh@math.toronto.edu